

REPORTS

slope of the straight line shows the spring constant of the waveguide to be 1.63×10^3 N/m. From this value we calculated the force exerted by *C. graminicola* during the formation of the penetration hypha underneath the appressorium. Force exertion typically began 100 to 120 min after the formation of mature—that is, melanized—appressoria (determined by visual inspection with the light microscope) and reached a steady level after ~ 300 min (Fig. 4B). This level did not change for several hours. In 18 appressoria from four fresh preparations of conidia cultured onto four different waveguides, we measured a force of $16.8 \mu\text{N}$ (SD $\pm 3.2 \mu\text{N}$, range 8 to $25 \mu\text{N}$).

Earlier studies used various techniques to measure the turgor pressure within an appressorium (17, 18). Given that the force is applied to an average diameter of $2 \mu\text{m}$ of the surface (Fig. 3D), which is in good agreement with the size of the penetration hyphae of *C. graminicola* as shown by transmission electron micrographs (19), the pressure within the appressorium would be 5.35 MPa. By comparison, Money (20) calculated that the pressure of 8.0 MPa found in appressoria of *M. grisea* corresponds to a force of $8 \mu\text{N}$, assuming that the surface of the penetration peg in this fungus is $\sim 1 \mu\text{m}^2$. These forces should be sufficient to breach the cuticle and epidermal cell wall of mono- and dicotylous plants (18).

In addition to allowing precise determination of vertical forces exerted by single appressoria on an underlying surface, the waveguides have a relaxation time of less than 1 s and so may be used to monitor dynamic processes. Data obtained in this way may help to analyze the effect of antipenetrants, for example, chemical agents that interfere with melanin biosynthesis or the biogenesis of fungal cell walls. The elasticity of the waveguide can easily be varied by using different types of elastomers (21), allowing measurements of forces down to the nanonewton range.

References and Notes

- E. C. Oerke, H. W. Dehne, F. Schönbeck, A. Weber, *Crop Production and Crop Protection* (Elsevier, Amsterdam, 1994).
- J. C. De Jong, B. J. McCormack, N. Smirnov, N. J. Talbot, *Nature* **389**, 244 (1997).
- R. J. Howard and B. Valent, *Annu. Rev. Microbiol.* **50**, 491 (1996).
- K. Mendgen, M. Hahn, H. Deising, *Annu. Rev. Phytopathol.* **34**, 367 (1996).
- Y. Kubo et al., *Appl. Environ. Microbiol.* **62**, 4340 (1996).
- J. D. Walton, *Plant Physiol.* **104**, 1113 (1994).
- A. Otto, *Phys. Stat. Sol.* **26**, K99 (1968).
- E. Kretschmann and H. Raether, *Z. Naturforsch.* **23A**, 2135 (1968).
- S. Herminghaus and P. Leiderer, *Appl. Phys. Lett.* **54**, 99 (1989).
- C. R. Lavers, *Thin Solid Films* **289**, 133 (1996).
- J. R. Sambles, G. W. Bradbery, F. Yang, *Contemp. Phys.* **32**, 173 (1991).
- W. Hickel and W. Knoll, *Acta Metall.* **37**, 2141 (1989).
- S. Herminghaus, C. Bechinger, W. Petersen, P. Leiderer, *Opt. Commun.* **112**, 16 (1994).
- PDMS M30.000 was obtained from Sigma.
- C. Bechinger, K.-F. Giebel, M. Schnell, P. Leiderer, H. B. Deising, M. Bastmeyer, data not shown.
- Colletotrichum graminicola* (Cesati) Wilson [teleomorph *Glomerella graminicola* (Politis)] was cultivated on 5% oatmeal medium, solidified with 1.2% agar. Cultures were incubated at room temperature under black-light lamps (Philips TL-D 36W/08). Conidia of three to five acervuli were suspended in distilled water and washed by repeated centrifugation to remove the germination self-inhibitor [B. Leite and R. L. Nicholson, *Exp. Mycol.* **16**, 76 (1992)]. The wild-type isolate of this fungus (CgM2) was obtained from R. L. Nicholson.
- N. P. Money and R. J. Howard, *Fung. Genet. Biol.* **20**, 217 (1996).
- R. J. Howard, M. A. Ferrari, D. H. Roach, N. P. Money, *Proc. Natl. Acad. Sci. U.S.A.* **88**, 11281 (1991).
- D. J. Politis and H. Wheeler, *Physiol. Plant Pathol.* **3**, 465 (1973).
- N. P. Money, *Can. J. Bot.* **73**, S96 (1995).
- S. Herminghaus, M. Riedel, P. Leiderer, M. Bastmeyer, C. Stürmer, *Appl. Phys. Lett.* **70**, 22 (1997).
- We thank M. A. Cahill for helpful comments on the text. Supported by grants from Deutsche Forschungsgemeinschaft (FOR 216/3), Optikzentrum Konstanz, and Fonds der Chemischen Industrie (M.B.).

24 May 1999; accepted 29 July 1999

Formation of Cycloidal Features on Europa

Gregory V. Hoppa,[†] B. Randall Tufts, Richard Greenberg, Paul E. Geissler

Cycloidal patterns are widely distributed on the surface of Jupiter's moon Europa. Tensile cracks may have developed such a pattern in response to diurnal variations in tidal stress in Europa's outer ice shell. When the tensile strength of the ice is reached, a crack may occur. Propagating cracks would move across an ever-changing stress field, following a curving path to a place and time where the tensile stress was insufficient to continue the propagation. A few hours later, when the stress at the end of the crack again exceeded the strength, propagation would continue in a new direction. Thus, one arcuate segment of the cycloidal chain would be produced during each day on Europa. For this model to work, the tensile strength of Europa's ice crust must be less than 40 kilopascals, and there must be a thick fluid layer below the ice to allow sufficient tidal amplitude.

Stress due to tidal deformation may drive global tectonics and the formation of linear features on Europa (1–6). However, the formation of the long chains of arcuate lineaments (or cycloids) on Europa has eluded

Lunar and Planetary Laboratory, 1629 East University Boulevard, University of Arizona, Tucson, AZ 85721–0092, USA.

[†]To whom correspondence should be addressed. E-mail: hoppa@lpl.arizona.edu

explanation. These features have several arcuate segments, each ~ 100 km in length. The Voyager spacecraft observed an abundance of cycloidal ridges (called “flexi” in the nomenclature of the International Astronomical Union) at high southern latitudes (1, 7, 8), at which location the spacecraft's observing geometry and the photometric conditions favored visibility (Fig. 1).

The Galileo spacecraft has observed cycloidal features of different morphologic types. The

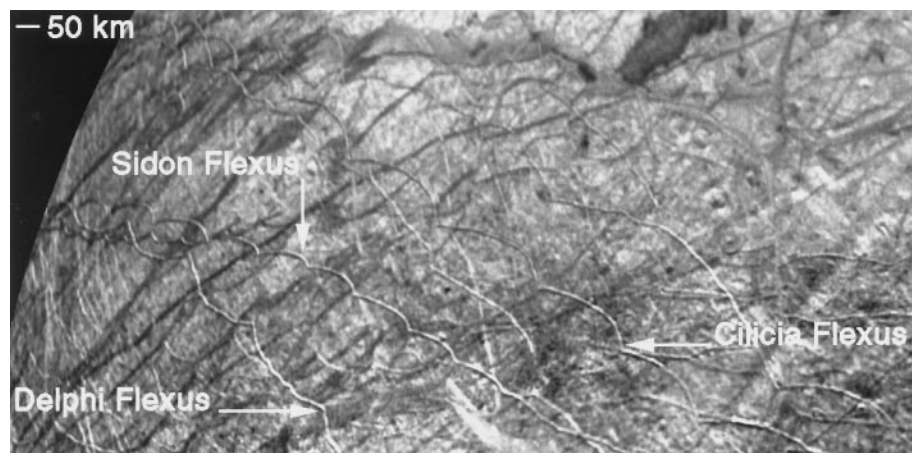


Fig. 1. Cycloidal ridges near Europa's south pole as viewed by the Voyager spacecraft (58°S, 166°W).

REPORTS

most primitive form of cycloidal feature is observed as a crack or trough (Fig. 2). These features appear not to have undergone any subsequent modification. Cycloidal features are more commonly observed in high-resolution Galileo images as double ridges (Fig. 3) [class 1 in Greenberg *et al.*'s (6) taxonomy], including those imaged by Voyager. Double ridges are the most common form of tectonic feature observed on the surface of Europa. If double ridges evolve from cracks in the ice, as proposed by all ridge formation models for Europa (6, 9–11), then the presence of cycloidal double ridges suggests that their shape represents the shape of the initial crack. Other arcuate features show evidence of lithospheric dilation or spreading of the crust (Figs. 3 and 4). Examples of arcuate features that have been pulled apart include wedge-shaped bands (12, 13) and Thynia Linea (14). Even the enormous strike-slip fault Astypalaea Linea may have been initiated as a cycloidal crack. Improved observation of the surface of Europa has provided evidence that cycloidal features are not restricted to any portion of the satellite. Previous models for the formation of cycloidal and other arcuate features depended on compression and thrust faulting (3, 7), including an analogy to island arcs on Earth (15). Galileo observations of these features show no evidence of compression or subduction along them (Figs. 2 and 3). Here we show how cycloidal features may form as tension cracks, with their form being controlled by the diurnal variation of tides (16).

As Europa orbits Jupiter, the amplitude and orientation of its tidal bulge vary with an 85-hour period due to Europa's orbital eccentricity. The consequent diurnal stress variations were computed (6) with a model that assumes an ice shell on top of a global ocean, which allows a ~30-m change in tidal amplitude over 42.5 hours (6). The magnitude of the tidal stress is proportional to $\mu(1 + \nu)/$

$(5 + \nu)$, where μ is the shear modulus and ν is the Poisson ratio. For water ice, plausible values are $\mu = 3.52 \times 10^9$ Pa and $\nu = 0.33$ (17). On the basis of this model, the stress field for any location on Europa at any point during its orbit can be computed.

Cycloidal cracks may form in response to Europa's tides in the following way: When the tensile strength of ice is reached, a crack forms perpendicular to the local direction of the tensile stress and begins to propagate. Because diurnal tidal stress changes, cracks propagate across an ever-changing stress field, in both amplitude and orientation. Thus, propagation can follow a curving path until it reaches a place and time where the tensile stress is insufficient to continue the propagation (Fig. 5). The propagation may be dormant until a few hours later, when the stress at the end of the crack once again exceeds the strength. At that time, propagation continues in a direction perpendicular to the new orientation of tensile stress. The shape of the crack then has a cusp, because the orientation of the tidal stress field changes substantially during the period when the crack is inactive.

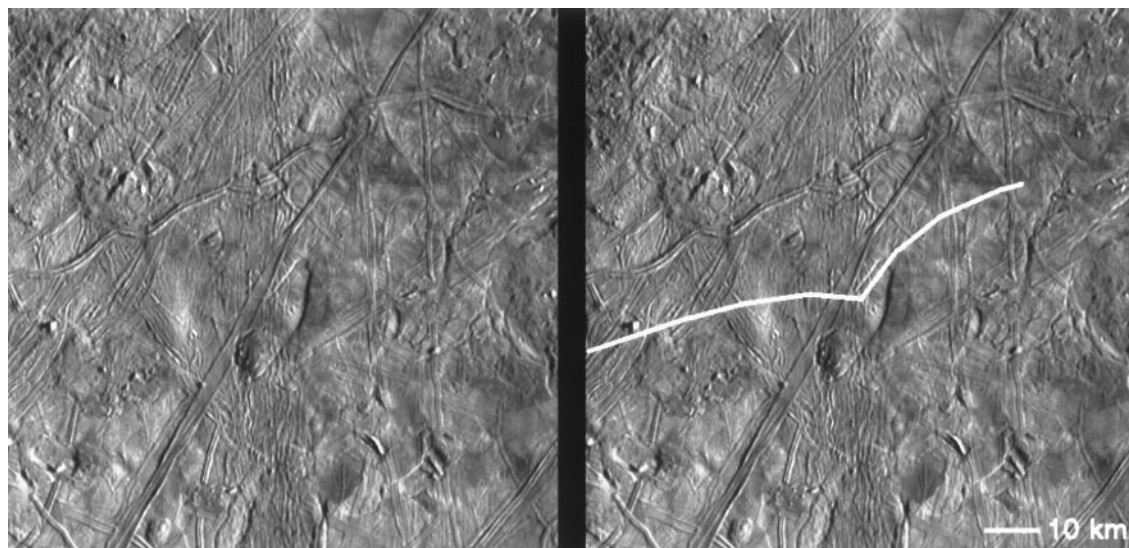
In addition to the amplitude and elastic moduli, three additional parameters are required to model cycloidal features quantitatively: (i) the crack initiation strength, which is the magnitude of the tensile stress required to initiate cracking; (ii) the crack propagation strength, which is the magnitude of the stress below which crack propagation halts; and (iii) the horizontal crack propagation speed. The maximum diurnal tensile stress for Europa is ~40 kPa. However, most regions of the surface are not stressed so much (6). Because cycloidal features have been observed at numerous locations on Europa, we assume a crack initiation strength of 25 kPa, which would allow crack formation to be widely distributed. We assume that the crack propagation strength is 15 kPa,

given that a crack is already initiated and fits the observed geometries of cycloidal features. Crack propagation stops when tensile stress drops below 15 kPa. Finally, we adopt horizontal crack propagation of 3 km/hour, for which the rotating orientation of the diurnal stress field generates curvature similar to that observed. This speed is also consistent with the formation of cusps spaced between 75 and 150 km, as observed; however, this speed is much lower than that of elastic cracks, which travel



Fig. 3. Cycloidal double ridges [class 1 in Greenberg *et al.*'s taxonomy (6)] viewed in the northern hemisphere of Europa (60°N, 80°W).

Fig. 2. Example of a cycloidal crack or trough observed near the crater Manannán (0°N, 238°W), with a key at the right highlighting the feature with a white line.



REPORTS

at a good fraction of the bulk speed of sound, so dissipation is probably important in the propagation process. Moderate variations in the strength (by ~ 8 kPa) and propagation speed can reproduce the diversity of observed cycloidal features at different orientations and locations.

In addition to the formation of the arcuate shape, the cusp, and the length of arcuate segments, other characteristics of cycloidal features may also be explained by this model. As shown in Fig. 1, some cycloidal features have arcuate segments that open northward (for example, Delphi Flexus) right next to features that open southward (for example, Sidon Flexus) (8). Our model explains the orientation of the cusps as a function of the direction of the crack propagation as follows: Features similar to Delphi Flexus (cusp northward) would form when cracks propagate westward in the southern hemisphere, whereas features similar to Sidon Flexus (cusp southward) would form when

cracks propagate eastward in the southern hemisphere. The opposite effect would take place in the northern hemisphere. Thus, the directions of crack propagation can be inferred for all observed cycloidal features.

Most arcuate features are skewed, so that there is a systematic change in the radius of curvature along the length of some cycloidal ridges. Good examples are seen in Sidon Flexus and Cilicia Flexus (Fig. 1). In our model, cycloidal cracks are similarly skewed if the crack propagation speed varies as a function of the tension. It is reasonable to expect the crack propagation speed to be proportional to the applied tension across the crack (that is, higher tensile stress would result in faster propagation). In this model, the crack initiates when stress levels are high (25 kPa), so crack propagation is faster and cracks are less curved at the beginning of each arcuate segment. As the tensile stress drops over the course of the orbit, the speed of the crack may also decrease and con-

sequently shorten the radius of curvature along the fracture. In this way, arcuate segments can be skewed, as observed on Europa.

This model also provides a mechanism for terminating the propagation of these cracks after several hundred kilometers (that is, several arcuate segments). The diurnal stress field on Europa varies as a function of latitude, longitude, and time (6). If a crack propagates into a region where the diurnal stress never reaches the strength of the ice, then cracking stops. Some cycloidal cracks may also fade into semi-linear features before the crack stops, if the crack is active for a very short period (< 10 hours) of the diurnal cycle. Additional regional geologic processes (that is, preexisting cracks that have not annealed) may also govern termination of crack propagation.

Finally, this model explains the large-scale curvature of cycloidal chains (for example, the concave upward curvature of the artificial chain shown in Fig. 5). Cycloidal features on Europa generally have such overall curvature (3, 7). This overall curvature results as a crack propagates to different longitudes. In the example shown in Fig. 5, the chain of cycloids formed during the first few orbits is aligned nearly in the east-west direction, because on average the tensile stress is in the north-south direction during the time of crack propagation. As the chain of cycloids moves eastward, the overall direction of the crack begins to turn northward. The change in overall bearing results from a change in the direction of the average tensile stress from the north-south direction to the northwest-southeast direction (6), thus causing the chain of cycloids to curve. Cycloidal lineaments on Europa curve in a sense consistent with our model.

Diurnal tidal variation provides a plausible explanation for the formation of cycloidal features on Europa. It reproduces many of the major characteristics associated with cycloidal features, including (i) the cycloidal segments, (ii) the cusps, (iii) the distances between cusps, (iv) the orientation of the cusps, (v) the skewness along cycloids, (vi) the termination of cycloidal features, and

Fig. 4. Extensional wedge-shaped bands (shown as darker features) (15°S , 195°W) were probably initiated as cycloidal cracks.

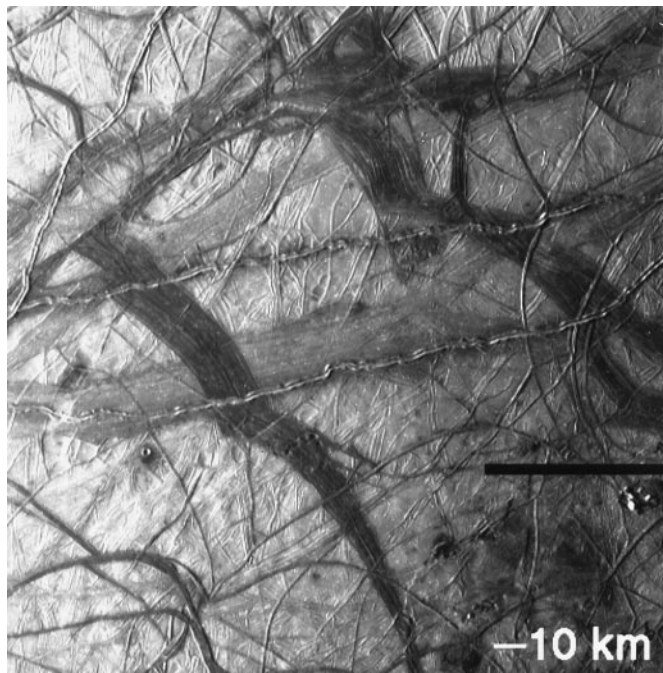
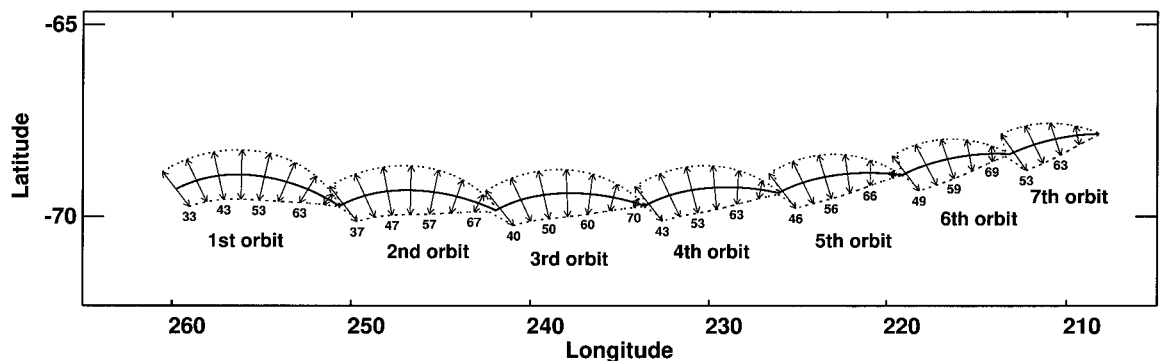


Fig. 5. Model of cycloidal crack formation on Europa. The arrows represent the amplitude and orientation of the tensile stress; the numbers below the arrows indicate the hours of the orbit. During the first orbit, cracking is initiated 33 hours after perijove. As propagation of the crack continues, the orientation of the tensile stress vector changes, causing the crack to change course. At 71 hours into the orbit, tension decreases to a point where crack propagation is no longer possible. The process repeats itself on subsequent orbits, making the characteristic cycloidal chain.



(vii) the large-scale curvature of the cycloidal chains. Cracks that are not cycloidal must have propagated faster or originated from a different stress pattern, such as that due to nonsynchronous rotation (4, 6, 18).

If Europa's water layer were solid down to the silicate layer without a substantial liquid layer (tens of kilometers thick), then diurnal tidal stress would be inadequate to fracture the surface because the amplitude of the tidal variation would be too small. The creation of cycloidal cracks requires a global ocean to generate substantial tidal stress over a diurnal cycle. Even so, the formation of cycloidal cracks may require that the ice be weak, because the maximum tidal stress is <40 kPa (<0.4 bar).

With so little stress, how deep can the cracks penetrate? Geologic evidence of lateral motion, dilation, and strike-slip motion on Europa suggests that cracks (including cycloidal cracks) from the surface penetrate down to a low-viscosity layer (13–15, 19, 20), possibly an ocean. However, with less than 40 kPa of tensile stress, as in the case of our model of cycloidal cracks, the tensile stresses are overwhelmed by the compressive hydrostatic overburden pressure at the depth of only ~65m (21). These cracks could be driven to greater depths by the insertion of liquid water (22, 23) or of material due to mass wasting (analogous to a wedge) (6, 23). Cracks may also go to greater depth because additional stress is concentrated at the base of the crack (18), but even that concentration is unlikely to drive a crack from the surface much deeper than ~1 km.

However, Crawford and Stevenson (24) noted that a thicker crust could crack all the way through if the crack initiates at the bottom of the ice layer and liquid water mitigates the overburden pressure. They noted that initiating a crack at the bottom would be difficult because the ice at the base would be warmer and thus less brittle than the colder ice at the surface. They also pointed out that even if a crack could start, it could propagate upward through only nine-tenths of the thickness of the ice layer (that is, up to the float line), but they speculated that additional forces would be needed, perhaps from gases dissolved in the water, to drive the crack through the remainder of the ice up to the surface.

Even if such an ad hoc process acted, it is unlikely that cracks could penetrate more than a few kilometers on Europa. At that depth, they might reach a ductile ice layer, which in principle could have served as the low-viscosity layer for lateral motion (19, 25). However, the association of cracks with ridge pairs suggests that the cracks penetrate to liquid water and not just ductile ice (6, 10, 11, 20). Thus our model implies that Europa's ice crust overlies liquid water and is thin enough that cracks go all the way through.

Cycloidal lineaments on Europa appear to

have formed in response to diurnal tides, a process that occurs quickly over the course of a few days, at a rate of one cycloid per European day (3.551 Earth days). This theory provides a specific time scale that is remarkably short for a major type of geological feature. Other icy satellites do not appear to have any analog to European cycloids, which suggests that only Europa has the unique characteristics necessary to form cycloidal features: A global ocean, substantial diurnal tidal stress, and a weak lithosphere.

References and Notes

1. B. A. Smith *et al.* *Science* **206**, 927 (1979).
2. S. J. Peale, P. Cassen, R. T. Reynolds, *ibid.* **203**, 892 (1979).
3. P. Helfenstein and E. M. Parmentier *Icarus* **53**, 415 (1983).
4. ———, *ibid.* **61**, 175 (1985).
5. A. S. McEwen, *Nature* **321**, 49 (1986).
6. R. Greenberg *et al.*, *Icarus* **135**, 64 (1998).
7. B. L. Lucchitta and L. A. Soderblom, in *Satellites of Jupiter*, D. Morrison, Ed. (Univ. of Arizona Press, Tucson, AZ, 1982), pp. 521–555.
8. M. C. Malin and C. C. Pieri, in *Satellites*, J. A. Burns and M. S. Matthews, Eds. (Univ. of Arizona Press, Tucson, AZ, 1986), pp. 689–717.
9. J. W. Head *et al.*, *J. Geophys. Res.*, in press.
10. S. D. Kadel *et al.*, *Lunar Planet. Sci. Conf. XXIX* [CD ROM] (1998).

11. E. P. Turtle *et al.*, *Eos* **79**, S202 (1998).
12. R. Sullivan *et al.*, *Nature* **391**, 371 (1998).
13. B. R. Tufts *et al.*, in preparation.
14. R. T. Pappalardo and R. Sullivan, *Icarus* **123**, 557 (1996).
15. M. Nolan and R. Greenberg, *Bull. Am. Astron. Soc.* **19**, 860 (1987).
16. G. V. Hoppa and B. R. Tufts, *Lunar Planet. Sci. Conf. XXX* [CD ROM] (1999).
17. P. H. Gammon, H. Klefte, M. J. Clouter, *J. Phys. Chem.* **87**, 4025 (1983).
18. A. C. Leith and W. B. McKinnon, *Icarus* **120**, 387 (1996).
19. P. M. Schenk and W. B. McKinnon, *ibid.* **79**, 75 (1989).
20. G. V. Hoppa *et al.*, *Icarus*, in press.
21. R. A. Smith, *J. Geol.* **17**, 223 (1976).
22. G. W. Ojkangas and D. J. Stevenson, *Icarus* **81**, 242 (1989).
23. B. R. Tufts, thesis, University of Arizona, Tucson (1998).
24. G. D. Crawford and D. J. Stevenson, *Icarus* **73**, 66 (1988).
25. M. P. Golombek and W. B. Banderdt, *ibid.* **83**, 441 (1990).
26. We thank W. McKinnon for his careful review and suggestions for improving this work, especially his insight into the propagation process, and the members and affiliates of the Galileo SSI team, led by M. Belton, for their comments and suggestions. Theoretical aspects of this work were supported by grant 347050 from NASA's Planetary Geology and Geophysics program.

28 April 1999; accepted 4 August 1999

Ultrasonic Deposition of High-Selectivity Nanoporous Carbon Membranes

Mark B. Shiflett¹ and Henry C. Foley²

Ultrasonic deposition creates a thin film of polymer on a tubular, macroporous, stainless steel support. Using polyfurfuryl alcohol as the nanoporous carbon precursor and a pyrolysis temperature of 723 kelvin, a membrane was prepared with the following permeances, measured in moles per square meter per Pascal per second: nitrogen, 1.8×10^{-12} ; oxygen, 5.6×10^{-11} ; helium, 3.3×10^{-10} ; and hydrogen, 6.1×10^{-10} . The ideal separation factors as compared to that for nitrogen are 30:1, 178:1, and 331:1 for oxygen, helium, and hydrogen, respectively.

Molecular separations are energy-intensive processes that can be used in a wide spectrum of areas, ranging from emerging biotechnologies to more classical fuels and chemicals production. The global move toward greener production is necessarily coupled with the need for more energy-efficient, and hence novel, separations. Molecular separations based on differences in molecular size and shape using ceramic membranes (1, 2) at ambient temperature are particularly intriguing, because these materials can conduct such separations with less energy.

This approach is particularly important for the removal of water from biotechnological broths in which the hydraulic load is high, but it is just as much an issue for gas separations such as the separation of nitrogen (N₂) from air, which is done by energy-intensive cryogenic distillation. Ceramic, as opposed to polymeric, membranes can operate under harsh conditions and at elevated temperatures (3), such as occur in reactive separations. Zeolites (4), sol-gels (5), and nanoporous carbons (NPCs) (6) are each candidate materials for the preparation of novel size-selective ceramic membranes.

Continuous nanoporous carbon membranes can be prepared as thin films supported on porous stainless steel by means of ultrasonic deposition (UD) of polyfurfuryl alcohol (PFA). These supported nanoporous carbon mem-

¹DuPont Central Research and Development, Experimental Station, Wilmington, DE 19880, USA. ²Center for Catalytic Science and Technology, Department of Chemical Engineering, University of Delaware, Newark, DE 19716, USA.